2026 IEEE/SICE International Symposium on System Integration (SII)
January 11-14, 2026. Cancún, México

Passivity-based Vs Momentum-residual-based external Disturbance Compensation for Closed Loop Torque Control : A comparative study

Martin Soucail, Mehdi Benallegue*, Mathieu Célérier, Bastien Muraccioli,
Thomas Duvinage, Helene Stefanelli, Rafael Cisneros-Limón

Abstract— **In torque-controlled robotic systems, external disturbances, whether from physical interactions or unmodeled dynamics, can significantly affect stability and performance. This paper investigates two different approaches for external disturbance compensation within closed-loop torque control frameworks: passivity-based compensation and residual-based compensation. The former leverages discrepancies between predicted and measured joint torques to estimate external forces, enabling fast reactive control. The latter relies on passivity theory to guarantee stability by shaping the system's energy exchange, making it robust to modeling uncertainties and sensor noise. We present the control formulations of both methods and evaluate them through experimental benchmarks in robotic tasks requiring compliant interaction. The theoretical and experimental results highlight the distinct strengths and limitations of each strategy in terms of responsiveness, stability, robustness, offering guidelines for selecting an appropriate disturbance compensation method depending on the application scenario.**

I. Introduction

Robot motion control is typically organized in a hierarchical architecture [1], where each layer receives reference inputs from the layer above and provides outputs to the layer below. At the lowest level, motor torque is regulated through current control. This current control layer receives desired current/torque values from a joint-level controller responsible for tracking joint trajectories. The joint-level controller, in turn, follows references from a task-space controller that ensures execution of the motion of the end-effector and other suimilar tasks. Around the top of the hierarchy, a task planner provides the desired task trajectories based on higher-level commands or goals. Other architectures are possibe, that may include even higher or lower level control layers [2]. In this paper we are interested in the layer that takes joint motion commands and converts them into torque references to be tracked.

This work includes results obtained from the project "Programs for Bridging the Gap between R&D and the Ideal Society (Society 5.0) and Generating Economic and Social Value (BRIDGE)/Practical Global Research in the AI × Robotics Services", implemented by the Cabinet Office, Government of Japan.

M. Soucail, M. Benallegue, M. Célérier, B. Muraccioli, T. Duvinage, H. Stefanelli, and R. Cisneros-Limón are with CNRS-AIST JRL (Joint Robotics Laboratory), IRL, National Institute of Advanced Industrial Science and Technology (AIST), Tsukuba 305-8560, Japan. martin.soucail@student-cs.fr, [mehdi.benallegue, mathieu.celerier, bastien.muraccioli, thomas.duvinage] @aist.go.jp, hstefanelli@student.ethz.ch, rafael.cisneros@aist.go.jp
* Corresponding author

There are two common ways to realize this layer. The first, usually termed *position control*, receives desired joint positions or velocities and uses joint-level feedback to generate the corresponding torques. It treats each joint as an independent subsystem, ignoring coupling, gravity, and external disturbances. Because these assumptions break down as soon as the joints are even partially back-drivable, the controller must rely on very high feedback gains. High gains make the robot's motion predictable and improve static and dynamic tracking while suppressing moderate disturbances. However, the lack of interaction awareness can be hazardous: if an obstacle suddenly blocks the planned path, the robot will still try to follow its reference, possibly damaging itself or its surroundings [3].

The alternative is *inverse-dynamics torque control*. This approach uses a whole-body dynamic model to compute the joint torques that achieve a given acceleration. Its accuracy depends on the fidelity of the model and on reliable estimates of gravity and external forces, yet the corresponding errors are usually smaller than those that undermine position control. The controller can therefore run with much lower gains. Low-gain regulation offers two key advantages. First, the robot becomes intrinsically compliant under unexpected contact, enhancing safety without an additional protective layer. Second, direct torque control allows precise shaping of interaction forces, simplifying the implementation of formal safety constraints. A torque-controlled robot can thus adapt its motion to unforeseen obstacles or disturbances, significantly reducing impact forces [4], [5]. These capabilities are especially valuable in tasks requiring delicate manipulation, such as assistive operations in healthcare environments.

Although compliance enhances safety, it diminishes tracking accuracy because the controller yields to disturbances. Furthermore, joint accelerations depend strongly on the accuracy of the dynamic model, so they are never followed perfectly. The resulting velocity drifts linearly, and the position drifts quadratically. Consequently, commanded accelerations cannot come from an open-loop trajectory planner. They must be generated by a closed-loop controller that updates the desired acceleration online to counteract kinematic drift. Even with such feedback, unmodelled friction, imperfect dynamics, and external forces bias the commanded acceleration, leading to tracking offsets and steady-state errors.

External–disturbance compensation in torque control has two major traditions in robotics. The first stems from disturbance observers (DOB) and reaction–force observers in mechatronics, which estimate and cancel unknown loads at

978-1-6654-5784-2/26/$31.00 ©2026 IEEE

high bandwidth [6]; in robotics this crystallized into momentum/residual observers used for sensorless external–torque estimation, collision detection, and safe reactions [7], [8], with recent variants improving robustness and bandwidth via sliding–mode designs [9]. The second tradition shapes the robot's energy exchange through passivity/impedance to guarantee stability under modeling errors and interaction uncertainty, notably for (flexible–joint) torque control [10]. Among these options, the two schemes studied here—passivity-based integral feedback and momentum–residual cancellation—strike a practical balance: they integrate cleanly with inverse dynamics, require only standard proprioception, and respectively offer (i) exact rejection of constant joint-space biases or (i) guaranteed dissipation of error energy, which we analyze and compare in this paper in terms of stability, passivity, and static and dynamic regimes. One approach explicitly estimates the joint torques produced by external forces and cancels them [11], [12], [13]; the estimator, based on generalized momentum and often called residual-based estimation, yields a first-order filtered approximation of the true disturbance torque and lumps modelling errors into the same residual term, so they are compensated as well. The second approach exploits passivity: it feeds back only the component of the deviation that carries non-zero error energy, leaving the passive part unchanged [14], [15], [5]; while it does not provide an explicit force estimate and is meaningful only in closed loop, it guarantees passivity with respect to the velocity error, which simplifies stability analysis when stacking several control layers. These two strategies combine theoretical guarantees with straightforward integration into existing inverse-dynamics torque loops using only standard proprioceptive sensing, making them the most relevant solutions to disturbance compensation.

a) Contributions: Building on these two paradigms, this paper provides a detailed side-by-side comparison of passivity-based and residual-based torque controllers, deriving their stability conditions, static and dynamic disturbance-rejection properties, and integration trade-offs. Both methods are implemented and benchmarked on a 7-DoF Kinova Gen3 in compliant trajectory tracking, with experiments demonstrating their dynamic performance. Section II introduces the two approaches; Section III analyzes stability and passivity; Section IV studies static and dynamic behavior; Section V reports experimental results; and Section VI concludes with key insights for controller selection.

II. Disturbance Compensation Approaches

We will first recall the robot's dynamics and notation, then detail each control law. This will set the foundation for the stability, static and dynamic analyses in the next sections.

A. Robot dynamics and notation

We consider an n-DoF rigid multi-body robot with configuration $\boldsymbol{q} \in \mathbb{R}^n$, velocity $\dot{\boldsymbol{q}}$, and acceleration $\ddot{\boldsymbol{q}}$. The joint-space dynamics under external torques is:

$$\boldsymbol{M}(\boldsymbol{q})\,\ddot{\boldsymbol{q}} + \boldsymbol{C}(\boldsymbol{q},\dot{\boldsymbol{q}})\,\dot{\boldsymbol{q}} + \boldsymbol{g}(\boldsymbol{q}) = \boldsymbol{u} + \boldsymbol{u}_d, \tag{1}$$

where $\boldsymbol{M}$ is the symmetric positive definite inertia Matrix, $\boldsymbol{C}$ is the Coriolis matrix such that $\dot{\boldsymbol{M}} - 2\boldsymbol{C}$ is skew-symmetric [16], $\boldsymbol{g}$ is the gravity term, $\boldsymbol{u}$ is the commanded torque, and $\boldsymbol{u}_d$ collects all unmodelled effects and disturbances.

Let's define the commanded joint acceleration $\ddot{\boldsymbol{q}}_c$. This acceleration is not the second derivative of a fixed, precomputed motion. Instead, it is computed online at each control cycle by the outer-loop controller (e.g., a whole-body QP or task-space feedback law) as a function of the current state of the robot and the task error. This design ensures that $\ddot{\boldsymbol{q}}_c$ continuously adapts to disturbances, model errors, and changing task objectives [15].

In order to realize this acceleration $\ddot{\boldsymbol{q}}_c$, the nominal inverse-dynamics torque, or *computed torque* is:

$$\boldsymbol{u}_c = \boldsymbol{M}\,\ddot{\boldsymbol{q}}_c + \boldsymbol{C}\,\dot{\boldsymbol{q}} + \boldsymbol{g} \tag{2}$$

Lat us define the velocity error

$$\boldsymbol{s} \triangleq \dot{\boldsymbol{q}}_c - \dot{\boldsymbol{q}}, \quad \text{with} \quad \dot{\boldsymbol{q}}_c(t) = \int_{t_0}^{t} \ddot{\boldsymbol{q}}_c(\iota)\,\mathrm{d}\iota. \tag{3}$$

Under the nominal control input $\boldsymbol{u} = \boldsymbol{u}_c$, the dynamics of $\boldsymbol{s}$ become: $\dot{\boldsymbol{s}} = -\boldsymbol{M}^{-1}\boldsymbol{u}_d$ which shows that the velocity error is directly driven by the external disturbance. Although the commanded acceleration is generated in closed loop, this open-loop treatment of the disturbance leads to steady-state tracking and static errors, as we will formally demonstrate in Section IV. Therefore, additional compensation mechanisms are needed to reject $\boldsymbol{u}_d$ and ensure accurate motion tracking.

The velocity error $\boldsymbol{s}$ is directly measurable from sensors and the known $\dot{\boldsymbol{q}}_c$, and can be the main feedback variable in the inner-loop torque control as shown hereinafter.

B. Passivity-based integral feedback

The first approach augments (2) with an integral feedback term proportional to $\boldsymbol{s}$:

$$\boldsymbol{u}_p = \boldsymbol{u}_c + \boldsymbol{L}\,\boldsymbol{s}, \quad \boldsymbol{L} \triangleq \boldsymbol{C} + \boldsymbol{K}, \quad \boldsymbol{K} \succ \boldsymbol{0}\ \text{(posit. def.)}, \tag{4}$$

where $\boldsymbol{K}$ may be constant or time or state-dependent as long as there is a minimal positive value for its eigenvalues.

C. Residual-based disturbance estimation

The second approach is to use the generalized-momentum residual to estimate the external joint disturbance torque $\boldsymbol{u}_d$ without using accelerations [17]. Define the generalized momentum $\boldsymbol{p} \triangleq \boldsymbol{M}(\boldsymbol{q})\,\dot{\boldsymbol{q}}$, whose dynamics, using $\dot{\boldsymbol{M}} - 2\boldsymbol{C}$ skew-symmetric and (1), is

$$\dot{\boldsymbol{p}} = \boldsymbol{u} + \boldsymbol{u}_d + \boldsymbol{C}^{\top}(\boldsymbol{q},\dot{\boldsymbol{q}})\,\dot{\boldsymbol{q}} - \boldsymbol{g}(\boldsymbol{q}). \tag{5}$$

The *residual* $\boldsymbol{u}_r \in \mathbb{R}^n$ is generated by the first-order filter

$$\boldsymbol{u}_r(t) = \boldsymbol{\Lambda}\left(\boldsymbol{p}(t) - \int_{t_0}^{t} \left[\boldsymbol{u} + \boldsymbol{C}^{\top}\dot{\boldsymbol{q}} - \boldsymbol{g} + \boldsymbol{u}_r\right](\iota)\,\mathrm{d}\iota - \boldsymbol{p}(t_0)\right), \tag{6}$$

Where $\boldsymbol{\Lambda}$ is a gain matrix such that $-\boldsymbol{\Lambda}$ is Hurwitz (stable). This yields the decoupled residual dynamics

$$\dot{\boldsymbol{u}}_r = -\boldsymbol{\Lambda}\,\boldsymbol{u}_r + \boldsymbol{\Lambda}\,\boldsymbol{u}_d. \tag{7}$$

giving these estimation error dynamics

$$\dot{\tilde{\boldsymbol{u}}}_d = \dot{\boldsymbol{u}}_d - \dot{\boldsymbol{u}}_r = -\boldsymbol{\Lambda}\,\tilde{\boldsymbol{u}}_d - \dot{\boldsymbol{u}}_d. \qquad \tilde{\boldsymbol{u}}_d \triangleq \boldsymbol{u}_d - \boldsymbol{u}_r. \quad (8)$$

If the gain $\boldsymbol{\Lambda}$ is high enough, this residual becomes a good estimate of the disturbance torque. This momentum-based construction avoids acceleration measurements and is independent of the particular torque controller used to produce $\boldsymbol{u}$. Closing the loop with the momentum residual yields the commanded torque

$$\boldsymbol{u}_b = \boldsymbol{M}\,\ddot{\boldsymbol{q}}_c + \boldsymbol{C}\,\dot{\boldsymbol{q}} + \boldsymbol{g} - \boldsymbol{u}_r, \quad (9)$$

which, replaced in the dynamics (1), gives

$$\dot{\boldsymbol{s}} \;=\; -\boldsymbol{M}^{-1}\,\tilde{\boldsymbol{u}}_d, \quad (10)$$

D. Similarity and gain choices

Developing (9) gives

$$\boldsymbol{u}_b = \boldsymbol{u}_c + \boldsymbol{\Lambda}\,\boldsymbol{M}\,\boldsymbol{s} - \boldsymbol{\Lambda}\int_0^t \big(\dot{\boldsymbol{M}}\,\boldsymbol{s}\big)\,\mathrm{d}v + \boldsymbol{\Lambda}\,\boldsymbol{p}(t_0), \quad (11)$$

which highlights a structural similarity with the passivity-based control law. In particular, the term $\boldsymbol{\Lambda}\,\boldsymbol{M}(\boldsymbol{q})\,\boldsymbol{s}$ acts as a proportional feedback on the velocity error $\boldsymbol{s}$, analogous to the $\boldsymbol{K}\,\boldsymbol{s}$ term in $\boldsymbol{u}_p = \boldsymbol{u}_c + (\boldsymbol{C}+\boldsymbol{K})\boldsymbol{s}$ from (4).

If we choose $\boldsymbol{\Lambda} \triangleq \boldsymbol{K}\,\boldsymbol{M}^{-1}$ with $\boldsymbol{K} \succ \boldsymbol{0}$, then $\boldsymbol{\Lambda}\,\boldsymbol{M}\,\boldsymbol{s} = \boldsymbol{K}\,\boldsymbol{s}$, so the proportional term in (11) coincides with the $\boldsymbol{K}\,\boldsymbol{s}$ term of the passivity law (4). The remaining contributions are the Coriolis term ($\boldsymbol{C}\,\dot{\boldsymbol{q}}$), the history integral $\int_0^t \dot{\boldsymbol{M}}(\boldsymbol{q},\dot{\boldsymbol{q}})\,\boldsymbol{s}\,\mathrm{d}t$, and the initialization term $\boldsymbol{p}(t_0)$. Since $-\boldsymbol{\Lambda} = -\boldsymbol{K}\,\boldsymbol{M}^{-1}$ is Hurwitz since the product of two symmetric positive–definite matrices has eigenvalues with positive real parts, the error dynamics are exponentially stable for $\boldsymbol{u}_d \equiv \boldsymbol{0}$, and the acceleration error remains stable even under constant disturbances as explained in the next sections.

To the best of our knowledge, such a gain choice has not been explicitly reported in the existing literature.

III. Stability analysis

A. Without disturbance

In this section, we analyze the stability properties of the two proposed inner-loop strategies, showing how each behaves when disturbances stop.

1) Exponential convergence of the passivity-based solution: In the disturbance-free case $\boldsymbol{u}_d \equiv \boldsymbol{0}$, substituting (4) into (1) and using $\boldsymbol{L} \triangleq \boldsymbol{C} + \boldsymbol{K}$ gives

$$\boldsymbol{M}\,\dot{\boldsymbol{s}} + \boldsymbol{L}\,\boldsymbol{s} = \boldsymbol{0}. \quad (12)$$

Consider the Lyapunov function

$$V(\boldsymbol{s}) = \tfrac{1}{2}\,\boldsymbol{s}^\top \boldsymbol{M}\,\boldsymbol{s} \quad (13)$$

Differentiating V along the trajectories of (12), and using the skew-symmetry of $\dot{\boldsymbol{M}} - 2\boldsymbol{C}$ yields $\dot{V} = -\,\boldsymbol{s}^\top \boldsymbol{K}\,\boldsymbol{s} \le -\,\alpha\,V.$, with $\alpha = \frac{\sigma_{\min}(\boldsymbol{K})}{\sigma_{\max}(\boldsymbol{M})} > 0$, which proves that $\boldsymbol{s}(t) \to \boldsymbol{0}$ globally exponentially with rate of at least α [15]. Moreover, from (12) we have

$$\dot{\boldsymbol{s}} = -\,\boldsymbol{M}^{-1}(\boldsymbol{C}+\boldsymbol{K})\,\boldsymbol{s}, \quad (14)$$

so $\dot{\boldsymbol{s}}(t)$ also converges to $\boldsymbol{0}$ exponentially.

2) Vanishing acceleration error for the residual compensation: When $\boldsymbol{u}_d \equiv \boldsymbol{0}$, the residual dynamics (7) reduce to

$$\dot{\boldsymbol{u}}_r \;=\; -\,\boldsymbol{\Lambda}\,\boldsymbol{u}_r \quad\Longrightarrow\quad \boldsymbol{u}_r(t) \;=\; e^{-\boldsymbol{\Lambda}\,(t-t_0)}\,\boldsymbol{u}_r(t_0), \quad (15)$$

so $\boldsymbol{u}_r(t) \to \boldsymbol{0}$ exponentially with rate $\sigma_{\min}(\boldsymbol{\Lambda})$. From the inner-loop error equation (10),

$$\boldsymbol{M}(\boldsymbol{q})\,\dot{\boldsymbol{s}} \;=\; -\,\tilde{\boldsymbol{u}}_d \;=\; \boldsymbol{u}_r \;\Longrightarrow\; \dot{\boldsymbol{s}}(t) \;=\; \boldsymbol{M}^{-1}(\boldsymbol{q}(t))\,\boldsymbol{u}_r(t). \quad (16)$$

If $\boldsymbol{M}(\boldsymbol{q})$ is boundedly invertible along the motion,

$$\|\dot{\boldsymbol{s}}(t)\| \le \|\boldsymbol{M}^{-1}(\boldsymbol{q}(t))\|\,\|\boldsymbol{u}_r(t)\|, \quad (17)$$

so the acceleration tracking error vanishes exponentially. However, since

$$\boldsymbol{s}(t) \;=\; \boldsymbol{s}(t_0) + \int_{t_0}^{t} \boldsymbol{M}^{-1}(\boldsymbol{q}(v))\,\boldsymbol{u}_r(v)\,\mathrm{d}v, \quad (18)$$

and since the integrand decays exponentially, $\boldsymbol{s}(t)$ converges to a (finite) constant $\boldsymbol{s}_\infty$.

3) Summary: In the passivity-based formulation, stability is established by tracking the *mechanical power* associated with the velocity error $\boldsymbol{s}$ through its time–integral, the Lyapunov storage function $V = \frac{1}{2}\,\boldsymbol{s}^\top \boldsymbol{M}\,\boldsymbol{s}$, which represents the kinetic energy of the error. In contrast, the residual-based method monitors the *external joint torque* $\boldsymbol{u}_d$ via its time–integral in the generalized momentum balance (7)–(15). In both cases, the integral quantity serves as the state of a first–order system whose decay rate determines the asymptotic behaviour: for the passivity-based loop, V decays exponentially, ensuring $\boldsymbol{s} \to \boldsymbol{0}$; for the residual loop, the disturbance estimate $\boldsymbol{u}_r$ decays exponentially, forcing $\dot{\boldsymbol{s}} \to \boldsymbol{0}$ while $\boldsymbol{s}$ converges to a constant offset.

B. Passivity Analysis of the Inner Loop

1) Motivation: We have seen that both controller were stable. However passivity provides an energy-based guarantee that is stronger than classical Lyapunov stability. A passive system cannot generate net energy, therefore any closed loop that starts with finite energy remains bounded for all time, which implies Lyapunov stability of the equilibrium. More importantly, the interconnection of two passive subsystems is also passive, so a passive inner torque loop can interact safely with passive environments, series elastic elements, or passive outer controllers without additional gain tuning. This property is crucial in robotics where the robot often exchanges power with uncertain or human partners.

2) Passivity property of the Passivity-Based Loop: The closed–loop error dynamics are

$$M(\boldsymbol{q})\,\dot{\boldsymbol{s}} + L(\boldsymbol{q},\dot{\boldsymbol{q}})\,\boldsymbol{s} = -\boldsymbol{u}_d, \quad (19)$$

We select the same error energy storage function $V(\boldsymbol{s}) = \frac{1}{2}\,\boldsymbol{s}^\top M(\boldsymbol{q})\,\boldsymbol{s}$ Its time derivative along (19) is

$$\dot{V} = -\,\boldsymbol{s}^\top K\,\boldsymbol{s} - \boldsymbol{s}^\top \boldsymbol{u}_d. \quad (20)$$

Define the supply rate $w = -\,\boldsymbol{s}^\top \boldsymbol{u}_d$. Because $-\boldsymbol{s}^\top K\,\boldsymbol{s} \le 0$, we get $\dot{V} \le w$ which proves that the mapping $\boldsymbol{u}_d \mapsto \boldsymbol{s}$ is passive with storage V.

3) Storage Function Analysis for the Residual-Based Inner Loop: the dynamics become

$$\dot{\boldsymbol{s}} = -M^{-1}\tilde{\boldsymbol{u}}_d. \tag{21}$$

If we consider the same kinetic-energy-like storage function V and we differentiate it along (21) and using the usual skew-symmetry relation between $\dot{M}$ and C yields

$$\dot{V} = \boldsymbol{s}^\top C(\boldsymbol{q},\dot{\boldsymbol{q}})\,\boldsymbol{s} - \boldsymbol{s}^\top \tilde{\boldsymbol{u}}_d. \tag{22}$$

which has indefinite sign. Hence the naive energy V_1 does not certify dissipation nor passivity of the mapping $\boldsymbol{u}_d \mapsto \boldsymbol{s}$.

We attempted another passivity storage for this loop but did not find one, though this does not imply none exists.

IV. Error dynamics of Inner Torque Loops

A. Static equilibria

1) Task dynamics: We analyse steady–state tracking errors under constant joint–space disturbance torques $\boldsymbol{u}_d$. The task is a set–point $\boldsymbol{x}_d$ tracked by a PD outer loop; the task Jacobian $\boldsymbol{J}(\boldsymbol{q})$ is assumed square and invertible in the operating region. The task dynamics are

$$\ddot{\boldsymbol{x}}_c = -\boldsymbol{D}_p\,\boldsymbol{e}_x - \boldsymbol{D}_d\,\dot{\boldsymbol{x}}, \qquad \boldsymbol{e}_x \triangleq \boldsymbol{x} - \boldsymbol{x}_d, \tag{23}$$

$$\ddot{\boldsymbol{q}}_c = \boldsymbol{J}^{-1}(\boldsymbol{q})\,\ddot{\boldsymbol{x}}_c - \boldsymbol{J}^{-1}\,\dot{\boldsymbol{J}}(\boldsymbol{q},\dot{\boldsymbol{q}})\,\dot{\boldsymbol{q}}, \tag{24}$$

with $\boldsymbol{D}_p, \boldsymbol{D}_d \succ \boldsymbol{0}$.

At static equilibrium we impose $\ddot{\boldsymbol{q}} = \dot{\boldsymbol{q}} = \dot{\boldsymbol{x}} = \boldsymbol{0}$; constant $\boldsymbol{u}_d$ and $\ddot{\boldsymbol{q}}_c$ and its time integral $\dot{\boldsymbol{q}}_c$ may be non-zero. The ss superscript means steady state value.

2) General steady–state relation: We write the inner torque as

$$\boldsymbol{u}_c \;=\; \boldsymbol{M}\,\ddot{\boldsymbol{q}}_c + \boldsymbol{C}\,\dot{\boldsymbol{q}} + \boldsymbol{g} + \boldsymbol{u}_{fb}, \tag{25}$$

where $\boldsymbol{u}_{fb}$ collects *only* the extra feedback beyond inverse dynamics. At static equilibrium we impose $\ddot{\boldsymbol{q}} = \dot{\boldsymbol{q}} = \dot{\boldsymbol{x}} = \boldsymbol{0}$, so $\boldsymbol{s} = \dot{\boldsymbol{q}}_c$, (1), (23) and (25) give

$$\boldsymbol{0} \;=\; \boldsymbol{M}\,\ddot{\boldsymbol{q}}_c^{\text{ss}} + \boldsymbol{u}_{fb}^{\text{ss}} + \boldsymbol{u}_d^{\text{ss}}. \tag{26}$$

Using $\ddot{\boldsymbol{x}}_c^{\text{ss}} = -\boldsymbol{D}_p\,\boldsymbol{e}_x^{\text{ss}}$ and (24),

$$\ddot{\boldsymbol{q}}_c^{\text{ss}} = -\boldsymbol{J}^{-1}\boldsymbol{D}_p\,\boldsymbol{e}_x^{\text{ss}} \overset{\boldsymbol{e}_x^{\text{ss}} = \boldsymbol{D}_p^{-1}\boldsymbol{J}\boldsymbol{M}^{-1}\left(\boldsymbol{u}_{fb}^{\text{ss}} + \boldsymbol{u}_d^{\text{ss}}\right)}{\Longrightarrow}. \tag{27}$$

Thus, the steady–state task error is fully determined by the *net* torque added to the feedforward torque, $\boldsymbol{u}_{fb}^{\text{ss}}$. Hereinafter we study three specializations.

3) Specializations:

a) Feedforward only: corresponding to pure inverse dynamics

$$\boldsymbol{u}_{fb} \equiv \boldsymbol{0} \quad\Longrightarrow\quad \boldsymbol{e}_x^{\text{ss}} = \boldsymbol{D}_p^{-1}\,\boldsymbol{J}\,\boldsymbol{M}^{-1}\,\boldsymbol{u}_d^{\text{ss}}. \tag{28}$$

showing that despite the task being tracked in closed loop, there is a steady-state error.

b) Passivity-based damping: The passivity based damping static feedback term is

$$\boldsymbol{u}_{fb} = \boldsymbol{K}\,\boldsymbol{s}, \Longrightarrow \boldsymbol{e}_x^{\text{ss}} = \boldsymbol{D}_p^{-1}\,\boldsymbol{J}\,\boldsymbol{M}^{-1}\left(\boldsymbol{K}\,\dot{\boldsymbol{q}}_c^{\text{ss}} + \boldsymbol{u}_d^{\text{ss}}\right), \tag{29}$$

and from (26),

$$\boldsymbol{0} = -\boldsymbol{M}\,\boldsymbol{J}^{-1}\boldsymbol{D}_p\,\boldsymbol{e}_x^{\text{ss}} + \boldsymbol{K}\,\dot{\boldsymbol{q}}_c + \boldsymbol{u}_d^{\text{ss}}. \tag{30}$$

Which gives that $\dot{\boldsymbol{q}}_c$ is constant and thus $\ddot{\boldsymbol{q}}_c^{\text{ss}} = -\boldsymbol{J}^{-1}\boldsymbol{D}_p\,\boldsymbol{e}_x^{\text{ss}} = 0$, we then get the equilibrium

$$\boldsymbol{e}_x^{\text{ss}} = \boldsymbol{0}, \qquad \dot{\boldsymbol{q}}_c^{\text{ss}} = -\boldsymbol{K}^{-1}\,\boldsymbol{u}_d^{\text{ss}}, \tag{31}$$

which yields perfect task tracking with the disturbance balanced by a non-zero commanded velocity.

c) Residual cancellation: In static, the estimated disturbance $\boldsymbol{u}_r$ matches perfectly the the actual one, $\boldsymbol{u}_d$

$$\boldsymbol{u}_{fb} = -\,\boldsymbol{u}_d \Longrightarrow \boldsymbol{e}_x^{\text{ss}} = \boldsymbol{0}, \qquad \ddot{\boldsymbol{q}}_c^{\text{ss}} = \boldsymbol{0}. \tag{32}$$

yelding a perfect task tracking as well.

4) Discussion: In steady state, the task error is completely determined by the feedback torque $\boldsymbol{u}_{fb}$ added to the inverse dynamics. Without feedback, the disturbance passes through the joint and task dynamics, creating an offset proportional to $\boldsymbol{u}_d$. Passivity–based damping balances the disturbance with a constant commanded velocity, yielding perfect task tracking while the robot itself remains at rest. Residual cancellation removes the disturbance directly in joint space, achieving zero error as well.

B. Perfectly Compensated Dynamic Disturbance

1) Motivation and Scope: Constant external torques are perfectly rejected by a residual–based estimator after convergence even during dynamic motions. Outside quasi–static conditions, however, real disturbances seldom remain constant, and the previous section showed that both residual and passivity corrections are bias–free when static. In dynamic case, the passivity loop does not cancel a constant torque, because it is designed to dissipate velocity–dependent interactions. This section derives the class of disturbances that *are* appropriately compensated by the passivity–based controller.

2) Closed–Loop Error Dynamics: Substituting (4) into (1) gives

$$M\,\dot{\boldsymbol{s}} + L\boldsymbol{s} = -\boldsymbol{u}_d. \tag{33}$$

3) Energy Analysis: Defining the velocity error energy Lyapunov function $V = \frac{1}{2}\boldsymbol{s}^\top M\boldsymbol{s}$, we get

$$\dot{V} = -\boldsymbol{s}^\top K\boldsymbol{s} - \boldsymbol{s}^\top \boldsymbol{u}_d. \tag{34}$$

The derivative is strictly negative if and only if we can write

$$\boldsymbol{u}_d = (N(t) + S(t))\,\boldsymbol{s}, \tag{35}$$

where $N(t)$ is a symmetric matrix such that $N(t) + K(t)$ is positive definite and $S(t)$ is a skew symmetric matrix ($S^\top(t) = -S(t)$). The orthogonal term is power conservative, giving $\boldsymbol{s}^\top S\boldsymbol{s} = 0$. Thus, no condition is required from S. In that case $\dot{V} < 0$ and $\boldsymbol{s} \to \boldsymbol{0}$, then perfect task tracking is recovered.

Equation (35) defines the full family of velocity-error-dependent disturbances that the passivity controller cancels exactly. Disturbances with a constant bias or position dependence may fall outside this matched subspace, so the passivity loop alone is not guaranteed to eliminate their effect.

We believe that a good way to understand what kind of disturbance applies to a robot is by running experiments,

V. Experimental results

This section presents experiments on the Kinova Gen3 robot, a 7-DoF manipulator arm. The robot was controlled with our open-source framework mc_rtc [1] and interfaced through Kinova's Kortex API, running at 1 kHz. Although the platform provides joint torque feedback that can enable high accuracy control [13], we deliberately ignored these measurements and relied only on the low-level current loop. This choice highlights the effect of unmodeled joint friction on task tracking. In particular, the Kinova Gen3 uses high-reduction harmonic drives, which generate substantial friction between the motors and joints, and this friction directly impacts the observed task error.

A. Experimental Procedure

The experiments were conducted under a consistent protocol, with the robot tested both in free motion and while carrying an unmodeled load. The Kinova Gen3 was first initialized in Position Control mode, then smoothly switched to Torque Control after 3 seconds. It was commanded to move to the starting point of a vertical circular trajectory of radius 25 cm, after which the end effector was tasked with tracking this trajectory at an angular velocity of $2\,\mathrm{rad}\cdot\mathrm{s}^{-1}$. This speed corresponds to the maximum feasible motion within the robot's safety limits when carrying the load.

The task gains were set to stiffness $\boldsymbol{D}_p = 60\boldsymbol{I}$ and damping $\boldsymbol{D}_d = 15.5\boldsymbol{I}$. To ensure both smoothness and uniqueness of the QP solution, we also included a posture task with a weight 10,000 times smaller than the main task.

For the inner-loop evaluation, we first compare pure inverse dynamics (ID) against its Passivity-Feedback-augmented variant (ID+PF), before contrasting the two disturbance–compensation schemes: passivity-based feedback (PF) and external torque estimation (ET).

B. Motion without external disturbances

We first executed the task without introducing external disturbances or additional modeling errors, but also without performing dynamic parameter identification or compensating for joint friction. The motion was carried out both with and without passivity feedback.

Due to inherent joint friction, the high speed of the task and modeling inaccuracies, the tracking was not perfect when using direct inverse dynamics alone. We then compared the performance with passivity-based feedback. The gains of the feedback were set to :

$$\boldsymbol{K} = 15\boldsymbol{M} + 10\boldsymbol{I}. \tag{36}$$

The mass-matrix term compensates the inertia-related component, so links closer to the end effector require lower corrective torque, while the identity term accounts for effects independent of inertia, such as friction.

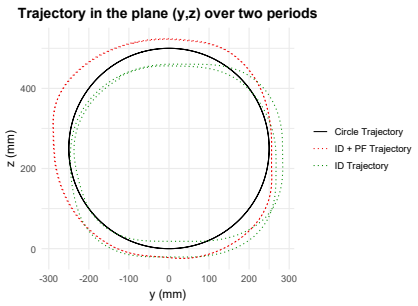

Fig. 1: End-effector trajectory in the (y, z) plane, without external disturbances, over two periods with just the ID or the ID + PF in comparison to the expected circle trajectory.

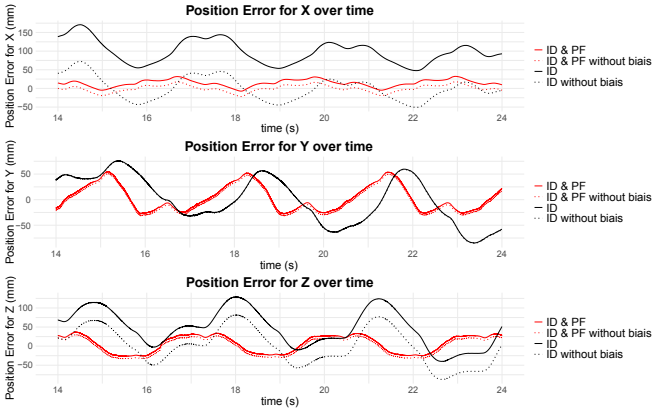

Fig. 2: Position tracking error in the case without external disturbances, with and without PF.

Figure 1 shows the tracked trajectory in both cases. While both controllers exhibit tracking errors, they do so differently: simple ID produces a downward bias, whereas ID+PF overshoots the radius. However, this plot does not convey the timing of the trajectory. The difference between the controllers becomes clearer in the error time plots of Figure 2, where the passivity-based feedback consistently reduces the tracking error, as also reflected in Table I. Furthermore, when the biases are removed, we see that PF reduces its variations over time.

This experiment demonstrates that, in the nominal case of current control with high-reduction gears, passivity-based feedback effectively compensates for friction and modeling errors, particularly at high speeds.

1) Motion with unmodeled load: The second experiment consisted of attaching a 1.25 kg weight to the arm at the End-

[1] https://jrl-umi3218.github.io/mc_rtc/index.html

TABLE I: Table of RMS values for position errors without external perturbations

	x-RMSE (mm)	y-RMSE (mm)	z-RMSE (mm)
ID	103.3	45.2	67.3
ID + PF	17.2	25.5	23.1

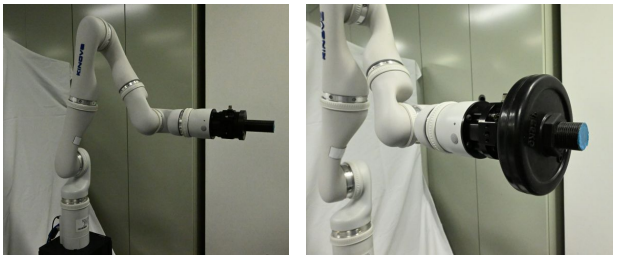

(a) Robot arm (b) Arm with added weight

Fig. 3: Configuration for the experiment.

Effector, without including this load in the robot model. This additional mass was significant relative to the robot's payload and overall mass distribution, and firmly secured using a dedicated mounting component, as shown in Figure 3.

Without PF, the controller applies torques as if the added weight were absent, leading to a dramatic drop in performance, as illustrated by the blue trajectory in Figure 4. In contrast, when PF is activated, the trajectories closely resemble those obtained without any attached weight, highlighting its ability to mitigate the impact of unmodeled payloads.

This effect is illustrated in Figure 5, which compares the tracking errors with and without additional weight, both under PF. The results show that the extra load was largely absorbed by the passivity-based compensation, while the remaining tracking imperfections are attributable to the same dynamic disturbances present in both cases.

C. Comparison Passivity Feedback and Residual-Based External Torque Estimation

In this section, we compare the two feedback methods: passivity-based feedback and residual-based external torque compensation. The same task was executed with the unmodeled load, and comparable gains were set as :

$$\boldsymbol{K} = 15\boldsymbol{M}, \qquad \boldsymbol{\Lambda} = 15\boldsymbol{I}, \tag{37}$$

so that both controllers yield the same instantaneous feedback term proportional to the velocity error $\boldsymbol{s}$. The only difference then arises from the Coriolis-related contributions and the history terms of the residual estimator, as detailed in Section II.

Unsurprisingly, we obtained very similar results from both loops, as illustrated in Figures 6 and 4 (red & green trajectories), and numerically confirmed in Table II.

D. On the similarity of both practical performances

All tested scenarios, including variations in gains and the introduction of additional disturbances, confirmed that both passivity-based and residual-based compensation yield

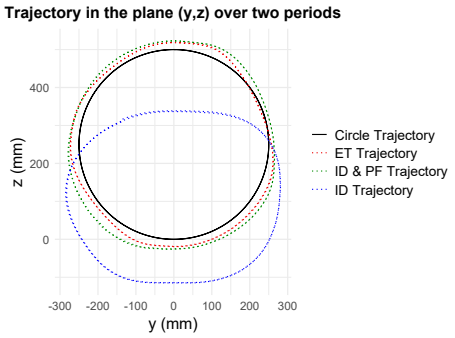

Fig. 4: End-effector trajectory in the (y, z) plane, under unmodeled load, over two periods with just the ID, the ID & PF and the ET in comparison to the expected circle trajectory.

Fig. 5: Position tracking error comparing the case with and without unmodeled load, both running with ID + PF.

similar tracking performance. This equivalence aligns precisely with the theoretical prediction that, for matched gains, both methods compensate the same velocity–error component. Unfortunately, cases where their conceptual differences would be expected to become prominent, such as under large, high-velocity errors or non–velocity-dependent disturbances, could not be executed safely on the available lightweight hardware. Hence, the choice between controllers should be guided primarily by their theoretical guarantees, such as the passivity property discussed in (**??**), rather than by measurable performance differences in this setup.

VI. Discussion and Conclusion

We presented a side-by-side theoretical and experimental comparison of passivity-based and residual-based distur-

TABLE II: Table of RMS values for position errors under unmodeled load

	x-RMSE (mm)	y-RMSE (mm)	z-RMSE (mm)
PF with Identity Gain	6.84	20.5	21.1
External Torque Estimation	8.6	18.0	15.9
Inverse Dynamic without PF	103.4	71.1	173.0

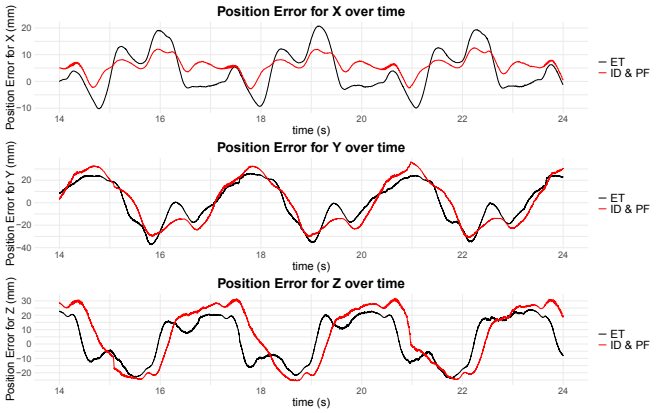

Fig. 6: Position tracking error under unmodeled load comparing the case with PF and with External Torque compensation.

bance compensation within inverse-dynamics torque control. Both approaches were examined in depth—covering stability, passivity, and their behavior under static and dynamic disturbances with an experimental validation on a 7-DoF torque-controlled arm. When tuned with comparable gains, their measured performance is nearly identical, which is expected since both controllers act on the same underlying velocity-error signal. However, their internal mechanisms and theoretical guarantees differ, particularly in scenarios involving large errors and high velocities.

From the experimental results and theoretical analysis, the main distinction arises from how each method treats the decomposition of a disturbance torque into components that do or do not contribute to the time derivative of the error energy. The passivity-based controller reacts only to the component of the disturbance that injects energy into the velocity error, deliberately ignoring energy-neutral components; this ensures that no net energy is introduced into the closed loop, guaranteeing passivity and thus robust stability when interacting with uncertain environments. In contrast, the residual-based controller aims to estimate and cancel the *entire* disturbance torque, including energy-neutral components, thereby preserving exact kinematic tracking even when the disturbance do not affect the energy balance.

This distinction has direct implications for method selection. In most applications, stability margins and predictable interaction behavior take precedence, making passivity-based compensation the safer choice. However, in situations close to safety-critical limits — such as imminent collisions, joint-limit approaches, or constrained tasks where tracking error must remain minimal, full disturbance rejection becomes more important than strict passivity. In such cases, the residual-based method can be advantageous, as it does not disregard disturbance components that are invisible to the passivity energy balance yet still cause kinematic drift.

In future work, we plan to investigate hybrid strategies that dynamically combine both approaches. A torque-control architecture could employ passivity-based compensation during nominal task execution to ensure robust stability, and seamlessly switch to residual-based compensation when approaching safety limits or executing precision-critical phases of a task. This would enable simultaneous exploitation of passivity guarantees for predictable interaction and full disturbance rejection when kinematic accuracy is paramount. We plan also to expand the comparison by crafting experiment specifically targeted to display a difference in behavior and to emphasize the specific effect of each approach, notably using he frequency domain and power logging.

REFERENCES

[1] R. Brooks, "A robust layered control system for a mobile robot," *IEEE Journal on Robotics and Automation*, vol. 2, no. 1, pp. 14–23, 1986.

[2] D. Kortenkamp, R. Simmons, and D. Brugali, *Robotic Systems Architectures and Programming*. Cham: Springer International Publishing, 2016, pp. 283–306.

[3] R. Kikuuwe, T. Yamamoto, and H. Fujimoto, "Velocity-bounding stiff position controller," in *2006 IEEE/RSJ International Conference on Intelligent Robots and Systems*. IEEE, 2006, pp. 3050–3055.

[4] A. Albu-Schäeffer, O. Eiberger, M. Grebenstein, S. Haddadin, C. Ott, T. Wimböck, S. Wolf, and G. Hirzinger, "Soft robotics: From torque feedback controlled lightweight robots to intrinsically compliant systems," *IEEE Robotics and Automation Magazine*, vol. 15, pp. 20–30, 01 2008.

[5] M. Benallegue, R. Cisneros, A. Benallegue, A. Tangui, A. Escande, M. Morisawa, and F. Kanehiro, "On compliance and safety with torque-control for robots with high reduction gears and no joint-torque feedback." in *Proc. of IEEE/RSJ Int. Conf. on Intelligent Robots and Systems*, 2021, pp. 6262–6269.

[6] K. Ohnishi, M. Shibata, and T. Murakami, "Motion control for advanced mechatronics," *IEEE/ASME transactions on mechatronics*, vol. 1, no. 1, pp. 56–67, 2002.

[7] A. De Luca and R. Mattone, "Sensorless robot collision detection and hybrid force/motion control," in *Proceedings of the 2005 IEEE international conference on robotics and automation*. IEEE, 2005, pp. 999–1004.

[8] S. Haddadin, A. Albu-Schaffer, A. De Luca, and G. Hirzinger, "Collision detection and reaction: A contribution to safe physical human-robot interaction," in *2008 IEEE/RSJ International Conference on Intelligent Robots and Systems*. IEEE, 2008, pp. 3356–3363.

[9] G. Garofalo, N. Mansfeld, J. Jankowski, and C. Ott, "Sliding mode momentum observers for estimation of external torques and joint acceleration," in *2019 International Conference on Robotics and Automation (ICRA)*. IEEE, 2019, pp. 6117–6123.

[10] C. Ott, A. Albu-Schaffer, A. Kugi, and G. Hirzinger, "On the passivity-based impedance control of flexible joint robots," *IEEE Transactions on Robotics*, vol. 24, no. 2, pp. 416–429, 2008.

[11] H. Sadeghian, L. Villani, M. Keshmiri, and B. Siciliano, "Task-space control of robot manipulators with null-space compliance," *IEEE Transactions on Robotics*, vol. 30, no. 2, pp. 493–506, 2013.

[12] M. Celerier, B. Muraccioli, M. Benallegue, Y. Hu, R. C. Limón, H. Kaminaga, and G. Venture, "Explicit compliance and safety on torque controlled robots for physical interaction," Apr. 2025, working paper or preprint. [Online]. Available: https://hal.science/hal-04922493

[13] B. Muraccioli, M. Celerier, M. Benallegue, and G. Venture, "Demonstrating a control framework for physical human-robot interaction toward industrial applications," in *Proceedings of Robotics: Science and Systems*, Los Angeles, USA, June 2025.

[14] J.-J. E. Slotine and W. Li, "On the adaptive control of robot manipulators," *The international journal of robotics research*, vol. 6, no. 3, pp. 49–59, 1987.

[15] R. Cisneros, M. Benallegue, A. Benallegue, M. Morisawa, H. Audren, P. Gergondet, and F. Kanehiro, "Robust humanoid control using a qp solver with integral gains." in *Proc. of IEEE/RSJ Int. Conf. on Intelligent Robots and Systems*, 2018.

[16] M. Bjerkeng and K. Y. Pettersen, "A new coriolis matrix factorization," in *2012 IEEE International Conference on Robotics and Automation*, 2012, pp. 4974–4979.

[17] A. De Luca, A. Albu-Schaffer, S. Haddadin, and G. Hirzinger, "Collision detection and safe reaction with the dlr-iii lightweight manipulator arm," in *2006 IEEE/RSJ International Conference on Intelligent Robots and Systems*, 2006, pp. 1623–1630.